

See discussions, stats, and author profiles for this publication at: <https://www.researchgate.net/publication/372309040>

An efficient skin cancer detection and classification using Improved Adaboost Aphid–Ant Mutualism model

Article in *International Journal of Imaging Systems and Technology* · July 2023

DOI: 10.1002/ima.22932

CITATIONS

13

2 authors:



Renith G

SRM Institute of Science and Technology

10 PUBLICATIONS 49 CITATIONS

SEE PROFILE

READS

249



Senthilselvi Ayothi

SRM Institute of Science and Technology



96 PUBLICATIONS 978 CITATIONS

SEE PROFILE

RESEARCH ARTICLE

WILEY

An efficient skin cancer detection and classification using Improved Adaboost Aphid–Ant Mutualism model

G. Renith  | A. Senthilselvi 

Department of CSE, SRM Institute of Science and Technology, Chennai, Tamilnadu, India

Correspondence

G. Renith, Research Scholar, Department of CSE, SRM Institute of Science and Technology, Ramapuram, Chennai, Tamilnadu, India.

Email: renithprem@gmail.com

Abstract

Skin cancer is the most common deadly disease caused due to abnormal and uncontrolled growth of cells in the human body. According to a report, annually nearly one million people are affected by skin cancer worldwide. To protect human lives from such life-threatening diseases, early identification of skin cancer is the only precautionary measure. In recent times, there already exist numerous automated techniques to detect and classify skin lesion malignancies using dermoscopic images. However, analyzing the dermoscopic images becomes an arduous task due to the presence of troublesome features such as light reflections, illumination variations, and uneven shape and dimension. To address the challenges faced during skin cancer recognition process, in this paper, we proposed an efficient intelligent automated system to detect and discriminate the dermoscopic images into malignant or benign. The proposed skin cancer detection model utilizes the HAM10000 dataset for evaluation. The dermoscopic images acquired from the HAM10000 dataset are initially preprocessed to enhance the quality of image and thus making it fit to train the classifier. Afterward, the most significant image patterns are extracted by the AlexNet architecture without any loss of detailed information. Later on, the extracted features are inputted to the proposed Improved Adaboost-based Aphid–Ant Mutualism (IAB-AAM) classification model to discriminate the images into malignant and benign categories. The proposed IAB-AAM approach witnessed extensive enhancement in classification accuracy. The enhanced performance is attributed by integrating the AAM optimization concept with the IAB model. By comparing the performance of the proposed IAB-AAM with other modern methods in terms of different evaluation indicators namely accuracy, precision, specificity, sensitivity, and f-measure, the efficiency of the proposed IAB-AAM technique is analyzed. From the experimental results, it is known that the proposed IAB-AAM technique attains a greater accuracy rate of 95.7% in detecting skin cancer classes than other compared approaches.

KEYWORDS

AlexNet architecture, Aphid–Ant Mutualism, detection, Improved Adaboost, pre-processing, skin cancer

1 | INTRODUCTION

One of the death-causing diseases is skin cancer, which is caused by the enhancement of cells in the body. In the human body, various classes of cancer exist and among them, skin cancer is a rapidly growing cancer, which is caused due to several factors such as viruses, physical activity, environmental changes, alcohol usage, smoking, allergies, and so on.¹ In general, skin cancer is separated into three categories namely squamous cell, basal cell, and melanoma. The squamous cells are seen in few places of the body and are commonly found in the outermost cells of dark people.² The basal cells are the lowermost layer cells and it is one of the least serious classes commonly occurring in fair people.³ Skin cancers are the high prevalence disease that appeared on the skin. Commonly, skin cancer is developed on the outermost layers of skin and initially appeared as swelling. The early identification of skin cancer is necessary to prevent deaths from fatal cancer.⁴ According to the histopathology view, skin cancer had an irregular structure with different levels of nucleus, cytoplasm, and chromatin.⁵ Skin cancers are categorized into melanoma and non-melanoma skin cancer. The most dangerous class of skin cancer is considered malignant melanoma, which leads to a higher proportion of patient's death through the late identification of pathology. Melanoma is one of the significant types of skin cancer that is appeared on the skin as a dark spot.⁶ Skin cancer is diagnosed by examining the biopsy and physical appearance. The biopsy is the simplest approach for diagnosing skin cancer and this process is unreliable and arduous.⁷

Recently, dermoscopic and macroscopic are the non-invasive instruments that help dermatologists in the diagnosis of skin cancer.⁸ The dermoscope is one of the devices utilized for acquiring lesions by skin images. Therefore, the device employed for identifying the vascular elements is named the dermoscope, which is a common microscope with crucial magnification and lens quality.⁹ The image obtained from the dermoscope is termed dermoscopic images. The effective detection of dermoscopic images needs four phases: artifacts exclusion, lesion segmentation, classification, and feature extraction.¹⁰ Various classes of computer-aided diagnosis systems are utilized to detect cancer, for the past few years.^{11–14} The conventional computer vision algorithm is utilized as the classifier for extracting a larger number of characteristics like texture, size, color, and shape for detecting cancer.¹⁵ Early detection and accurate diagnosis of skin cancer will assist the proper medical treatment and healing process as well as prevents the worse effects of the skin cancer.¹⁶ There are a few challenges in detecting skin cancer, which are distributed to variations in

image sources and types. If the skin cancer is not identified in the initial phases, it can affect the lungs, cerebrum, bones, and liver as well as it becomes very complicated to identify.¹⁷ The primary challenge in skin cancer is various shapes and sizes of images could not give the correct result of the detection.¹⁸ Color illuminations also make a few challenges possessing its factors such as light rays, reflections, and color texture.¹⁹ This paper develops an efficient automated and intelligent skin cancer detection system to detect and classify the cancer classes precisely. The following points present the key contributions of this paper.

- A novel Improved Adaboost-based Aphid–Ant Mutualism (IAB-AAM) classification model is proposed to accurately detect and discriminate the skin cancer dermoscopic images into distinct categories (i.e., benign or malignant).
- The main reason behind the enhanced classification accuracy is due to parameter optimization process. The parameters of the IAB model are fine-tuned using the AAM optimization algorithm.
- The most relevant image features are extracted without losing any detailed information from the preprocessed images through AlexNet architecture.
- Investigating the effectiveness of the proposed classification model over other state of art approaches in terms of diverse evaluation indicators such as accuracy, precision, specificity, sensitivity, and f-measure.

The rest of the paper is as follows, Section 2 explains the literature survey of various research articles obtained from different researchers. Section 3 describes the proposed methodology of IAB-AAM and the result part is illustrated in Section 4. Section 5 describes the conclusion part.

2 | RELATED WORKS

Numerous techniques are used to detect and classify skin cancer, and here we presented few techniques for our analysis.

Khamparia et al.²⁰ established a transfer learning-driven deep internet of health and things (TLDDIoHT) framework to classify and detect skin cancer. The features were extracted from the skin lesion images by using Inception V3, ResNet50, VGG19, and SqueezeNet architectures for enhancing the classification accuracy of skin cancer. The International Skin Imaging Collaboration (ISIC) image archive dataset was selected to categorize skin cancer as benign and malignant. Among 5000 images, only 3800 images were given for the training

process and the remaining 1200 images were used for the testing process. The performance metrics such as recall, accuracy, precision, and F1 score were applied for experimental analysis and the result showed high classification accuracy at the same time task processing time is high. The differential evolution-based artificial neural network (DE-ANN) approach for skin cancer detection and classification was illustrated by Kumar et al.²¹ The DE-ANN approach was employed to classify the skin cancer into cancerous or non-cancerous and the image segmentation method was applied for separating the heterogeneous image regions by fuzzy C-means clustering. The DE-ANN approach produced more false positives rates on detecting malignant skin lesions.

Tan et al.²² introduced enhanced particle swarm optimization (EPSO) to detect skin cancer. The skin cancer was classified into two namely malignant and benign skin lesions and for detection; three different datasets such as PH2, Dermofit Image Library, and Dermnet were employed. For image classification, 1300 images were selected for Dermofit Image Library, 200 images for PH2, and 152 images for Dermnet. The EPSO approach obtained less classification accuracy. Dorj et al.²³ elaborated a deep convolutional neural network (DCNN) for classifying skin cancer. For the classification of skin cancer, the RGB images and error correction output codes support vector machine (ECOC SVM) classifier were used. The AlexNet model was applied to the feature extraction and 3753 images were selected from the Internet. The parameters like accuracy, sensitivity, and specificity were employed for getting high performance rate to detect the skin cancer. The result showed that the accuracy and specificity rate was high when compared to the modern techniques. The skin cancer was not able to detect through smart phones.

To tackle multinomial skin lesion classification issues in categorizing fine grained variability, Khan et al.²⁴ introduced a new framework to localize and classify the lesion images into distinct categories. The localization process involves three diverse operations, which initially segment the lesion region from the dermoscopic images by removing irrelevant features using a 16-layer high dimension contrast transform (HDCT) and Convolutional neural network (CNN) strategy. Subsequently, the details of lesion part were fused through maximum mutual information (MMI) model. Finally, the extreme learning machine (ELM) classifier discriminates the feature vectors into separate classes accurately but it consumes more time during localizing the lesion areas. Mohakud et al.²⁵ presented a Convolutional neural network-based gray wolf optimization (CNN-GWO) algorithm to precisely detect the skin

cancer classes. The training time of CNN was enhanced by incorporating preprocessing pipeline. The hyper-parameters of CNN classifier were optimized through GWO algorithm to design a cost effective framework. The optimized CNN framework thus accurately detects and classifies the multiple diseased classes into relevant categories. The limitation of CNN-GWO approach was slow convergence ability to determine the optimal solution.

For accurate recognition of skin cancer in an earlier stage, Ali et al.²⁶ demonstrated a DCNN method, which correctly discriminates the malignant and benign images in the dataset more efficiently. With the intention to obtain an accurate classification result, the raw dermoscopic images acquired from HAM10000 dataset were fed into the kernel to remove artifacts. The dermoscopic images were augmented to increase the quantity of data, which help to increase the classification accuracy of the classifier. This approach effectively categorizes the dataset into malignant or benign but failed to distinguish malignant classes. Khan et al.⁸ developed an automatic melanoma cancer detection mechanism to properly classify the melanoma class from the nevus. It makes use of a Gaussian filter to eliminate the redundant noises from the images and then utilizes an improved k-means clustering process to extract the lesion part. Finally, to discriminate melanoma and nevus categories individually, the support vector machine (SVM) classifier was used. However, this method was not applicable to implement in large-scale datasets.

A review on skin cancer detection to explain where we are and the way to the future has been presented in Goceri.²⁷ Furthermore, CNN-based desktop applications and mobile applications developed to classify various skin diseases have been presented in Göçeri; Goceri and Karakas; and Aggrey et al.^{28–31} Besides, capsule-based deep networks have been proposed in recent works.^{11,32}

3 | PROPOSED METHODOLOGY

The difficulties associated with variations in image categories and sources cause detection of skin cancer a complicated task. It occurs due to the fact that each skin image sample is varied from the other in terms of skin tone and texture. To solve these problems, a new automated technique is presented in this paper to accurately detect malignant and benign skin lesions. This approach will help dermatologist to take preventive measures. The input images obtained from HAM10000 dataset initially go through preprocessing pipelines such as

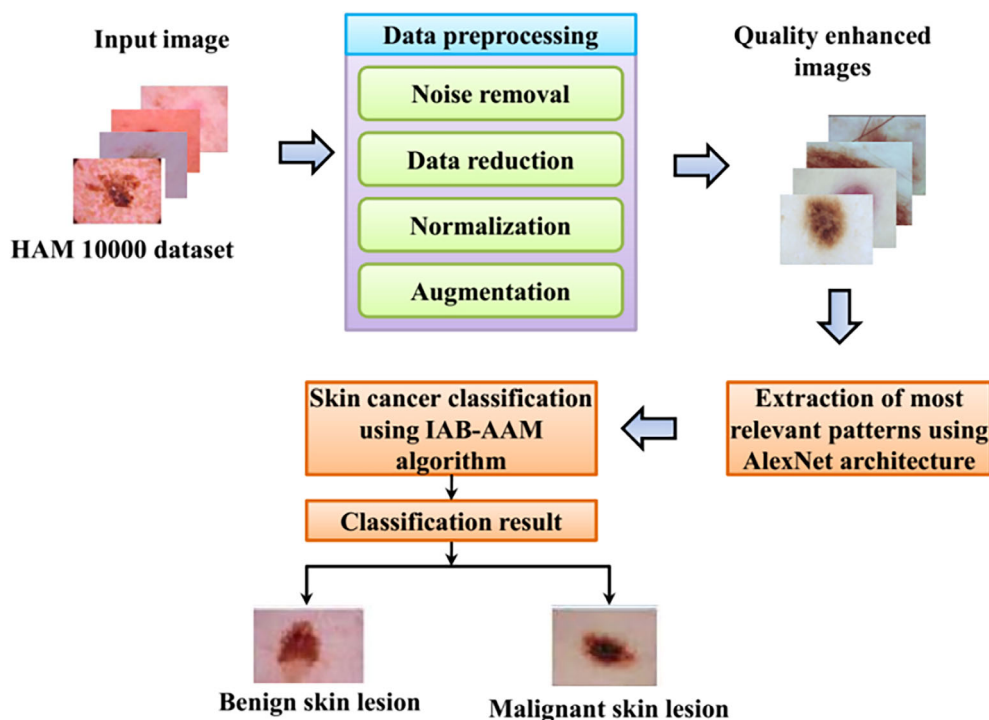


FIGURE 1 Architecture of proposed skin cancer detection module. IAB-AAM, Improved Adaboost-based Aphid–Ant Mutualism.

HAM10000 dataset	Malignant	Benign	Unknown lesions
	1113	6705	2197

TABLE 1 Dataset description.

noise removal, data reduction, normalization, and augmentation for the enhancement of image quality. Later on, the most relevant features from the preprocessed data are extracted through AlexNet architecture by removing the insignificant patterns. Finally, the IAB-AAM classifier discriminates the extracted dermoscopic images into benign or malignant. Figure 1 presents the framework of the proposed skin cancer detection technique.

3.1 | Dataset collection

The skin cancer images for this study are collected from the HAM10000 dataset. Collecting the skin cancer images is somewhat critical. This dataset comprises 10 015 images obtained from Australian and Austrian patients. Among these images, 1113 images are malignant, 6705 images are benign, and 2197 images are undisclosed lesions. In this dataset, the same lesion from different perspectives or different images of the same lesion from the same patient is compared. In the validation and test set, the images that are far away or low clarity are removed but these images are used in the training set. In data preparation, factors like feature selection, feature

engineering, data cleaning, dimensionality reduction, and data transform finalize the training dataset. The data in the HAM10000 dataset are given in Table 1.

3.2 | Data pre-processing phase

The data augmentation process is utilized for enhancing the amount of data by modified copies without using new data obtained from the existing training data. The oversampling and data warping methods can increase the size of the training dataset and it will protect the model from the over-fitting problem.³³ Data preprocessing can improve the raw medical image by eliminating impulse noises, bubbles, and artifacts created on applying gel prior to taking dermoscopic images. The dermoscopic images also contain artifacts such as hairs, low contrast image, blur image, and color illumination images. Those artifacts and noises are eliminated from the original image for enhancing the classification rate. After removing all artifacts and noises from the images, the data minimization, feature extraction, augmentation, and data normalization steps are applied. Finally, the obtained data are converted into a numerical data format.

3.2.1 | Noise elimination

A comprehensive review of the denoising approaches applied with dermoscopy images can be found in Goceri.³⁴ Gaussian and median filtering may lead to blurring sharp-edge structures and image details. However, they are more efficient in terms of computational costs than the other denoising methods. Furthermore, their efficiency can be increased by implementing them with appropriate parameters. Therefore, in this work, median blurring and Gaussian blurring filters have been implemented to remove all quantity of noises. The artifact reflections are classified and detected by using single-pixel with respect to Equation (1) as:

$$\{J(a,b > S_{P1})\} \text{ and } \{(J(a,b) - J_{average}(a,b)) > S_{P2}\} \quad (1)$$

where J and $J_{average}(a,b)$ represent image and average intensity, respectively. The threshold values are $S_{P1} = 0.87$ and $S_{P2} = 0.096$.³⁵ The imprinting activities are implemented for the artifact-identified area, which can separate the data from the artifacts. The noise in the pixel is mathematically expressed as:

$$S_r = S_{r0} + m \quad (2)$$

here m and S_{r0} are denoted as noise in the pixel and true value of pixel, respectively. If the mean of artifacts and noise values are zero, the mathematical form is changed into $S_r = S_{r0}$.

3.2.2 | Data minimization

The data minimization process can reduce the number of images from the raw images and then converted into a smaller volume. It is considered as a difficult task for getting a good classification rate from the dataset due to the presence of images with artifacts and noises, low contrast image, blur image, wounds with mole images, and color illumination images.

3.2.3 | Data normalization

The data normalization process can reduce the data uprightness, data redundancy, and also carried out unnecessary characteristics like deletion anomalies, update, and insertion. Some data normalization techniques are decimal scaling normalization, z-score

normalization, and min-max normalization. The objective of data normalization is as follows:

- The data normalization process will improve the coherence and cohesion for segmentation, data purification, high quality of data, and lead generation.

To normalize the dataset, it will be divided by 255 denoted as the grayscale value of the image. The dataset is normalized by using the z-score normalization method is given below:

$$W'_j = \frac{W_j - \mu}{\sigma} \quad (3)$$

here W'_j is the z-score normalized value. The mathematical form of standard deviation and mean values are given by:

$$\sigma = \sqrt{\frac{1}{(m-1)} \sum_{j=1}^m (W_j - \mu)^2} \quad (4)$$

$$\mu = \frac{1}{(m)} \sum_{j=1}^m W_j \quad (5)$$

where σ and μ are standard deviation and mean value, respectively.

3.2.4 | Augmentation

The data augmentation process is utilized for enhancing the amount of data by modified copies without using new data obtained from the existing training data. The oversampling and data warping methods can increase the size of the training dataset and it will protect the model from the over-fitting problem. The data are augmented by various augmentation parameters such as color shifting, rotation, mirroring, and random cropping to overcome the over-fitting issues. The parameters of data augmentation are as follows,

- Horizontal flip: The action of horizontal flip is the images flip to the horizontal direction.
- Height shift range: The images are shifted to a vertical direction by 0.2.
- Rotation range: The input data can be generated with rotation ranges from -10 to 10 .
- Width shift range: The images are shifted to a horizontal direction by 0.2.
- Zoom range: Zoom out or in 0.2 from the center.

3.3 | Feature extraction phase

One of the important methods that play a major role in image processing, for making it more manageable for further processing, is feature extraction. In this paper, a larger number of features are extracted, which assists in recognizing and identifying the larger numbers of the dataset. This paper employs AlexNet to minimize the dimensionality issues for further classification of skin disease. The detailed elaboration and mathematical description of AlexNet architecture are discussed below.³⁶

3.3.1 | AlexNet

The AlexNet design is extracted the dense and latent features from the skin data.³⁷ One of the forms of CNN is AlexNet design that gives the best performance results. The skin data are gathered from the Ham10000 dataset and it consists of noisy and missing values. The noise present in the skin data are in the terms of outliers, missing records, anomalies, redundant records and overlapping, and so forth. The noise is handled or else the proposed design produced false results as well as enhanced the false positive rate to a larger extent. The AlexNet design minimized the noise effect to a minimum level and automatically chose the relevant features. Then, AlexNet is employed for extracting the dense and hidden characteristics from the skin data. The AlexNet architecture consists of a pooling, fully connected, and convolution layer. AlexNet architecture consists of five convolutional layers, three max-pooling layers, and a dropout layer. The initial convolutional layer contains 96 neurons with 11×11 filter dimension, 4 strides, and its output feature map dimension is $227 \times 227 \times 3$. The second convolutional layer contains 256 neurons with 5×5 filter dimension, 1 stride, 2 padding, and its output feature map dimension is $27 \times 27 \times 256$. The third and fourth convolutional layers consist of 384 neurons with 3×3 filter dimension, 1 stride, 2 padding, and $13 \times 13 \times 384$ feature map dimension. The final convolutional layer contains 256 neurons with 3×3 filter size, 1 padding, and 1 stride. This layer's output feature map dimension is $13 \times 13 \times 256$. Each max-pooling layer contains similar 3×3 dimensioned filters and two strides with varied output feature map dimension as $27 \times 27 \times 96$, $13 \times 13 \times 256$, and $6 \times 6 \times 256$, respectively, for first, second, and third max-pool layers. The dropout layer with dropout rate 0.5 outputs feature map dimension $6 \times 6 \times 256$. The detailed explanations of every component are given below.

3.3.2 | Convolutional layer

One of the significant parts of CNN is the convolutional layer. This layer is utilized for attaining the latent and abstract characteristics, while the pooling layer is very helpful for getting higher level characteristics that minimized the difficulty of dimensionality. The skin data are transformed into 2D weekly data. The convolutional layer is utilized for acquiring the characteristics from 3D (three-dimensional data) and 1D (one-dimensional data). The convolution operations among the filters and shapes are explained through the below equation.

$$CONV(inp_{sh}, fil) = \sum_{j=1}^{o_i} \sum_{k=1}^{o_x} g_{jk} \quad (6)$$

In convolution, the learnable mechanism is expressed and followed as:

$$Z_{CONV}(Y_u^{gu}) = \vartheta \left(\sum_{gu=1}^{gu} X_u^{gu} \times Y_u^{gu} + c_u^{gu} \right) \quad (7)$$

From the above equation, the output feature map is represented by Y_u^{gu} , the bias and weight factors are represented by c_u^{gu} and X_u^{gu} , the rectified linear unit (ReLU) is denoted by ϑ .

3.3.3 | Pooling layer

The convolutional layers are utilized for extracting the lower-level features from the skin data. In the input data, a slight change will create a distant feature map. These modifications will occur due to flipping, rotation, and cropping of the input images. The signal processing methods are utilized for minimizing the feature maps resolution size. The pooling layer is one of the new concepts based on DL designs. The max-pooling method is adopted for minimizing the skin data's spatial dimensions. The mathematical expression of the max-pooling layer is calculated as:

$$z^n = MAX_{j,k} \in S(z_{j,k}) \quad (8)$$

The outcomes of the max-pooling operations are represented by z^n , the set of real numbers are denoted by S , and the k_{th} neuron and j_{th} convolutional layers are denoted by k and j .

3.3.4 | Activation layer

After the operation of convolution, the activation function is utilized for the extraction of feature maps. Tanh, sigmoid, leaky ReLU (LReLU), linear, and ReLU are the various activation functions in the literature. The ReLU functions overcome the vanishing and exploding gradient issues as well as increases the performance. The mathematical expression for the ReLU function is calculated and it is followed as:

$$\text{ReLU} = \text{MAX}(0, \text{VALUE}) \quad (9)$$

3.3.5 | Dropout layer

The Ensemble DL designs are presented to overcome the overfitting issue. The design is hard for maintaining several designs during training. The single neural networks are simulated the various architecture by dropout layers. Few neurons of the hidden layers are deactivated by the dropout layer to overcome the issues of overfitting.

3.3.6 | Flatten layer

After the execution of the operation, the feature map is transformed into ID data as well as passed to neural networks for differentiating the malicious and normal skin data. The extracted feature sets are acquired after the removal of noisy and overlapping values.

3.3.7 | Fully connected layer

The final layer of the AlexNet is fully connected and it extracted the global characteristics from the feature maps. It also compiled the flattened layer results for performing the last classification. The mathematical expression for this layer is calculated as follows:

$$g_p = \vartheta(X_u \cdot y_u + c_u) \quad (10)$$

The input feature vector is represented by y_u , the bias and weight factors are denoted by c_u and X_u , the ReLU function is denoted by ϑ , the final output is denoted by g_p .

3.4 | Skin cancer classification phase

Data classification is an indispensable step that makes use of extracted patterns from the ALEXNet architecture

to classify the images into benign or malignant categories. Based on the recognized patterns, the classification task is performed using a novel automated IAB-AAM classifier. To attain enhanced classification accuracy, the parameters of the IAB model are fine-tuned using the AAM optimization algorithm. A thorough explanation of the proposed classification approach is delineated in the following sub-sections.

3.4.1 | Improved Adaboost algorithm

The intrinsic properties of initial threshold values and input data samples can be determined by using an improved AdaBoost algorithm.³⁸ The ridge regression method prevents the data from the multi-collinearity problem. Due to the variance and bias, the prediction errors are divided into two different sub-components to avoid the multi-collinearity problem. The shrinkage parameter is applied to ridge regression for solving the multi-collinearity problem is expressed as:

$$\text{Ridge regression} = \underset{\alpha \in PQ}{\text{ArgMin}} \|y - B\alpha\|_2^2 + \gamma \|\alpha\|_2^2 \quad (11)$$

where γ is the shrinkage parameter and the Equation (11) can be denoted as the combination of penalty and loss component. In Equation (11), the first term is the least square term and the other term depicts the summation of coefficient α . The lasso regression can penalize the regression coefficient's absolute size and also enhance the accuracy rate is expressed as:

$$\text{Lasso regression} = \underset{\alpha \in PQ}{\text{ArgMin}} \|y - B\alpha\|_2^2 + \gamma \|\alpha\|_1 \quad (12)$$

The absolute values can be employed instead of using square values, which comprise a major difference in lasso regression compared with ridge regression. So the penalized parameter estimates turn into negligible condition and the estimates are zero when the applied penalty is large. The improved Adaboost algorithm follows some steps:

Step 1: Inputs are considered as the sequence of samples $(x_1, y_1), \dots, (x_t, y_t)$. Here, the total number of iterations and weak learners are represented as Y and the output $y \in T$.

Step 2: The values are initialized such as weight vector $v_t^d = E_d(i)$, iteration index $d = 1$, error rate $\tau_d = 0$, and distribution $E_d(i) = 1/t$.

Step 3: While $d \leq Y$

- a. The weak learner provides the appropriate distribution $q^{(d)} = \frac{v^{(d)}}{Z_d}$. Here W_{L_d} , Z_d , and $q^{(d)}$ represents weak

learner, normalization factor, and distribution, respectively.

- b. The lasso and ridge regressions are applied to the regression model $g_d(x) \rightarrow x$.
- c. The initial stage of the received signal is given by $k[m] = n[m] + w[m]$, which can be used for implementing the soft thresholding concept. Where $w[m]$ and $n[m]$ are denoted as Gaussian distribution noise factor and unknown signal, respectively. The soft thresholding is expressed as

$$\hat{N} = \begin{cases} k - \text{sgn}(k)R & \text{if } |k| \geq R \\ 0 & \text{if } |k| < R \end{cases} \quad (13)$$

- d. Calculate the error

$$h_d(i) = g_d(x_i) - y_i \quad (14)$$

- e. Calculate the error rate

$$\tau_f = \sum_{i \in q} q_i^{(d)} \quad (15)$$

where $q = \{i \mid |h_d(i) - \bar{h}_d| > \gamma \eta_d\}$, $i \in [1, t]$, \bar{h}_d , $\gamma \eta_d$, η_d , and γ are depicts expected value, robust threshold value, standard deviation, and relative factor, respectively.

- f. To initialize $\alpha_d = \tau_d / (1 - \tau_d)$.
- g. The contribution can be used to evaluate the final result

$$\beta_d = -\log(\alpha_d) \quad (16)$$

- h. Update the weight factors

If $i \in Q$ then $v_i^{(d+1)} = v_i^{(d)} \alpha_f$;
Else $v_i^{(d+1)} = v_i^{(d)}$

1. Finally set $d = d + 1$

Step 4: The term β_1, \dots, β_d is normalized. Let us assign $\sum_{d=1}^Y \beta_d = 1$ and the hypotheses output is given by

$$e_{hin}(x) = \sum_{d=1}^Y \beta_d e_d(x) \quad (17)$$

3.4.2 | Aphid–Ant Mutualism

Aphids are one of the major social insects belonging to the family Aphididae. Ants and aphids are lived together with same habits and they have different interaction by the surrounding environments.³⁹ One of the important zoological feminine is ants and it has three classes, namely male, queen, and female workers. The major phases of the AAM are colonies creation, generating the initial population, aphids fight, ant's evolution, and mutualism. Various steps are performed on population for identifying the global optimum and advancing the search mechanism.

Generation of initial population

AAM begins by the generating the random populations of O_{POP} individuals. Therefore, the population is separated into two classes, and they are ants and aphids. The populations of ants and aphids are expressed in the below equation:

$$\begin{aligned} APHID_{l,k} &= MC_k + \mathfrak{R} \times (VC_k - MC_k), l = 1, 2, \dots, o \\ ANT_{q,k} &= MC_k + \mathfrak{R} \times (VC_k - MC_k), q = 1, 2, \dots, n \end{aligned} \quad (18)$$

The upper and lower bounds of the kth variable is represented by VC_k and MC_k , the uniform random number is denoted by \mathfrak{R} , the lth aphid position in kth dimension is indicated by $APHID_{l,k}$, as well as the qth ants position in kth dimension is denoted by $ANT_{q,k}$.

Colonies creation

Ants and aphids are generated colonies for benefiting the mutualism in the nature. The aphid's populations are analyzed by utilizing the objective function as well as sorted the individuals ranking value. Ringleaders are chosen from populations to form predefined aphid colonies. The remaining aphids are known as weak aphids. The attraction of weak aphids and attraction to ant colonies are explained in the following subsection.

Attraction of weak aphids to colonies

The mth ring leader attraction power is computed and expressed as:

$$NA_o = 2 - \zeta P + 2 \times (\zeta P - 1) \times \frac{\frac{MAX_j\{Qs_j\} - Qs_o - 1}{\sum Qs_j}}{N_{COL} - 1} \quad (19)$$

In the initial population, total amount is indicated by N_{COL} , the objective of the oth ringleader is represented by Qs_j , the fitness of best ringleader is indicated by $MAX_j\{Qs_j\}$.

$$OD_o = RO\{NA_o \times N_{COL}\} \quad (20)$$

The number of aphids in *oth* colony is represented by OD_o .

Attraction of ants to colonies

The ants are attracted arbitrarily to *oth* colony is computed and it is expressed as:

$$NANT_o = RO\{NA_o \times O_{ANTS}\} \quad (21)$$

The total number of ants is represented by N_{ANTS} , the *oth* ringleader attraction power is denoted by NA_o .

Mutualism

In the AMM, various search methods are designed for updating the individual's position by the inspiration of mutualism within ants and aphids.

Exploitation stage

The ϕ is the parameter utilized for controlling the selected aphids as well as the best aphids utilizing the searching methods for propagating the characteristics in population.

$$APHID_{j,k}(u+1)^o = APHID_{j,k}(u)^o + \beta_1 \times \frac{\Re o}{u} \times (VC_k - MC_k) \quad (22)$$

The position of the j th aphid in k th dimension in $(u+1)$ th iteration on *oth* colony is represented by $APHID_{j,k}(u+1)^o$, the scaling parameter is denoted by β_1 , the current iteration number is denoted by u . The position of aphid in the current iteration is indicated by $APHID_{j,k}(u)^o$.

Exploration stage

The j th aphid position in k th dimension at $(u+1)$ th iterations on *oth* colony is computed and expressed as:

$$APHID_{j,k}(u+1)^o = ANT_{\Re}(u)^o + \alpha \times \Re o \mid (APHID_{j,k}(u)^o - ANT_{\Re}(u)^o) \mid \quad (23)$$

From the above equation, α and $\Re o$ signifies the normal and uniform random distribution that ranges from 0 to 1, respectively. The amount of pheromone minimizes in accordance with the rate of evaporation. At first iteration, the rate of evaporation is small (i.e., near to 0) and gradually enhances to 1. The following equation states the rate of evaporation:

$$P = \frac{T - 0.1}{\text{maximum Iteration}} \quad (24)$$

From the above equation, P indicates the evaporation rate of pheromone. The present and total number of iterations are designated by T and maximum Iteration, respectively.

Computational complexity

The computational complexity of AAM signifies functions that map the runtime of the algorithm. Therefore, Big O notation is employed as a prevalent technology, which is stated in the following expression.

$$O(\text{Complexity}) = O(\text{Initial}) + O(\text{Fitness determination as \& sort}) + O(\text{update the position}) \quad (25)$$

3.4.3 | Proposed IAB–AAM approach for accurate skin lesion classification

Figure 2 illustrates the working procedure of the proposed IAB–AAM classifier. The proposed classification model is inputted with the most significant patterns acquired from the ALEXNet architecture. It has a higher ability to learn dense and latent features of dermoscopic images. This extraction process helps the classifier to detect accurately the cancer classes (i.e., benign or malignant) with a shorter training time. Initially, the Adaboost module assigns threshold values on the basis of intrinsic properties of input images. The regression model namely ridge regression, lasso regression, and soft thresholding are constructed to resolve multicollinearity problems, minimize variability issues, and improve detection accuracy, respectively. Then the error rate is computed to determine whether the threshold value is robust. The weight vectors, which are updated by the module, are verified to make further classification decisions. If the achieved weights are not optimal, the optimization process is conducted through AAM optimization algorithm. Due to its enhanced searching strategies, it neglects premature convergence and converges to an ideal solution rapidly. Thus, the AAM algorithm fine-tunes the parameters of the IAB model and enhances the converging performance of the classifier efficiently. As a result, the proposed IAB–AAM model efficiently and accurately classifies the dermoscopic images of the HAM10000 dataset into two distinct categories as malignant skin lesions and benign skin lesions.

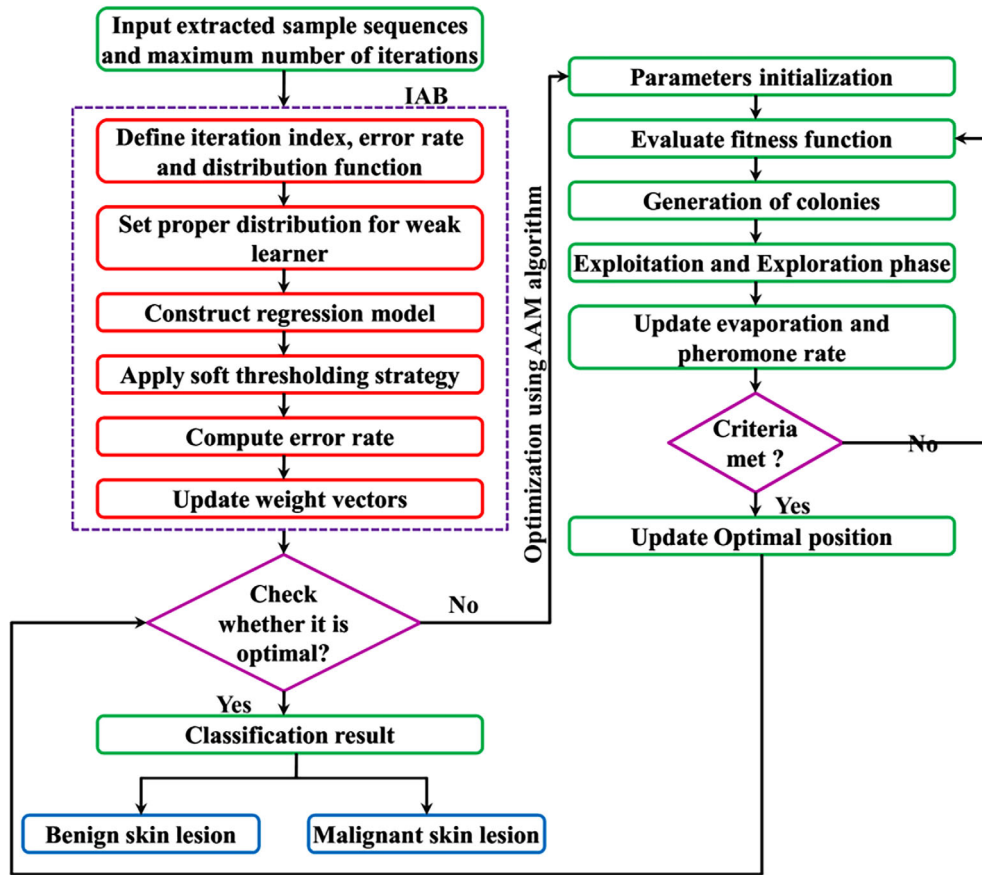


FIGURE 2 Flow diagram of the IAB-AAM approach. IAB-AAM, Improved Adaboost-based Aphid–Ant Mutualism.

TABLE 2 Parameter settings.

Parameters	Ranges
Total iteration	30
Learning rate	0.2
Shrinkage parameter	(0,1)
α	Rand (0,1)
β_1	0–1

4 | EXPERIMENTAL RESULTS

In this section, the skin cancer detection and classification performance of the proposed method is determined by evaluating various performance analyses debated in Table 2. The skin cancer images for this study are collected from the HAM10000 dataset. Here, 80% of the data are employed for training and the rest 20% are for testing the dataset.

4.1 | Parameter settings

Table 2 portrays the parameter settings of our proposed approach.

TABLE 3 Various evaluation indicators.

Measures	Formulas
Accuracy	$\frac{t_{pos} + t_{neg}}{t_{pos} + f_{pos} + t_{neg} + f_{neg}}$
Precision	$\frac{t_{pos}}{t_{pos} + f_{pos}}$
Specificity	$\frac{t_{neg}}{t_{neg} + f_{neg}}$
Sensitivity	$\frac{t_{pos}}{t_{pos} + f_{neg}}$
F-measure	$\frac{t_{pos}}{t_{pos} + \frac{1}{2}(f_{pos} + f_{neg})}$
Matthews correlation coefficient	$\frac{t_{neg} \times t_{pos} - f_{pos} \times f_{neg}}{(t_{pos} + f_{pos})(t_{pos} + f_{neg})(t_{neg} + f_{pos})(t_{neg} + f_{neg})}$

4.2 | Performance measures

To estimate the efficiency of the proposed method, various performance metrics are applied such as accuracy (A), precision (P), specificity (SP), sensitivity (Sen), F-measure, and Matthews correlation coefficient (MCC). The mathematical expression for each metric is given below. The true positive, true negative, false positive, and false negative are denoted as $t_{pos}, t_{neg}, f_{pos}, f_{neg}$, respectively, as mentioned in Table 3.

4.3 | Comparative analysis

The proposed IAB-AAM method points out the Analysis of accuracy and loss between testing and training represented in Figures 3 and 4. The proposed IAB-AAM method of accuracy and loss ratio is calculated for the alternate epochs. Due to increasing the epochs, the training and testing accuracy also maximized. However, the proposed IAB-AAM method attains minimal training and testing loss. In inaccuracy analysis, the training accuracy ratio is higher compared to the test accuracy. In loss analysis, the training loss ratio is lower compared with the test loss ratio. In machine learning, it is typical for the training accuracy to be a bit higher than the testing accuracy. This is because the model uses the training data to make predictions, so it is expected to perform slightly better on the training data.

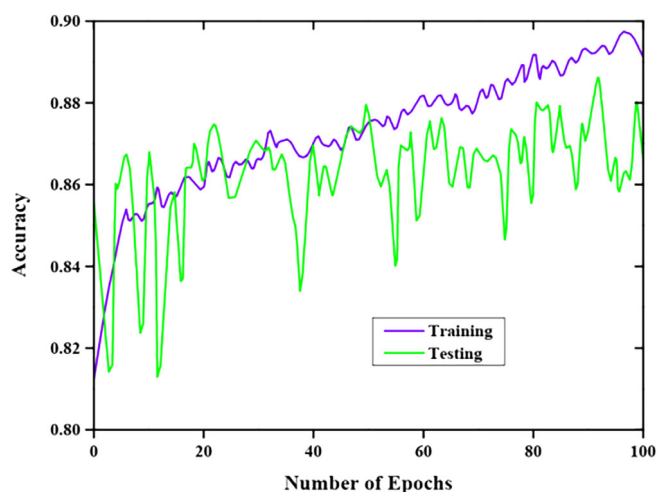


FIGURE 3 Training and testing accuracy analysis.

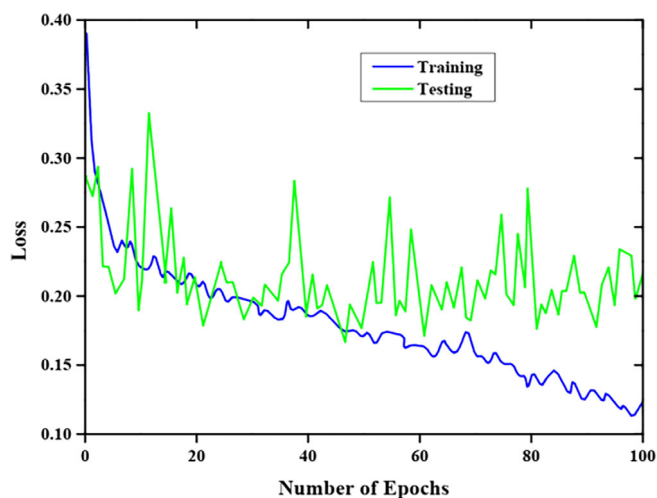


FIGURE 4 Training and testing loss analysis.

Detection of skin cancer and classification are various methods for analyzing the accuracy ratio illustrated in Figure 5. When compared to the DCNN, differential evolution-based artificial neural network (DE-ANN), convolutional neural network-based gray wolf optimization (CNN-GWO), and SVM that the proposed method obtained a higher accuracy rate. The proposed IAB-AAM method can detect and classify skin cancer more efficiently with an accuracy of 95.7%.

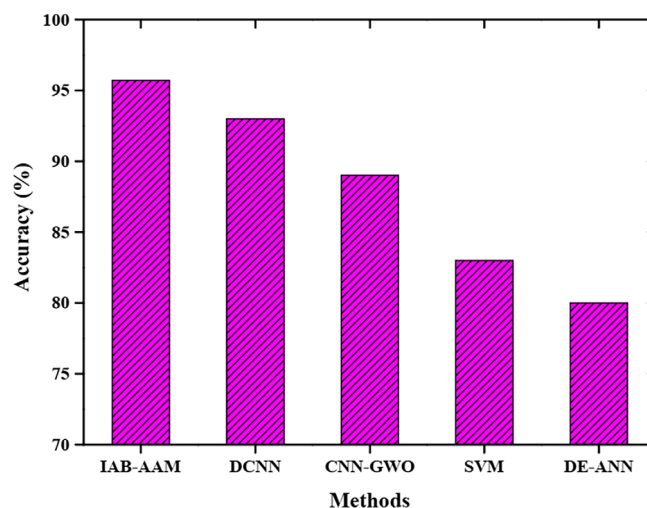


FIGURE 5 Accuracy analysis. CNN-GWO, convolutional neural network-based grey wolf optimization; DCNN, deep convolutional neural network; DE-ANN, differential evolution-based artificial neural network; IAB-AAM, Improved Adaboost based Aphid-Ant Mutualism; SVM, support vector machine.

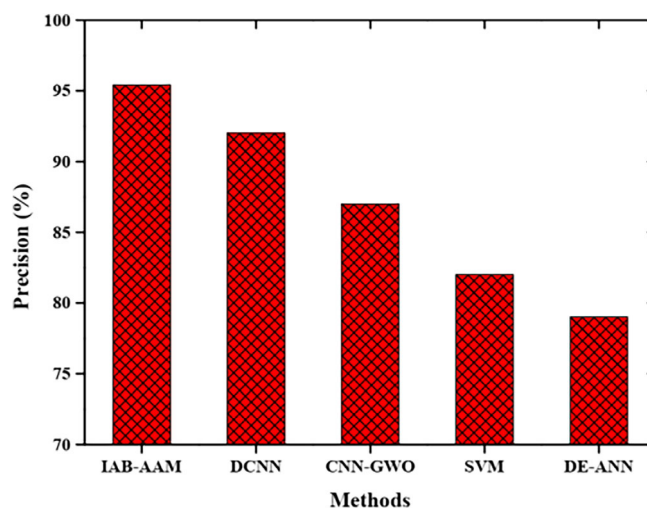


FIGURE 6 Precision analysis. CNN-GWO, convolutional neural network-based grey wolf optimization; DCNN, deep convolutional neural network; DE-ANN, differential evolution-based artificial neural network; IAB-AAM, Improved Adaboost based Aphid-Ant Mutualism; SVM, support vector machine.

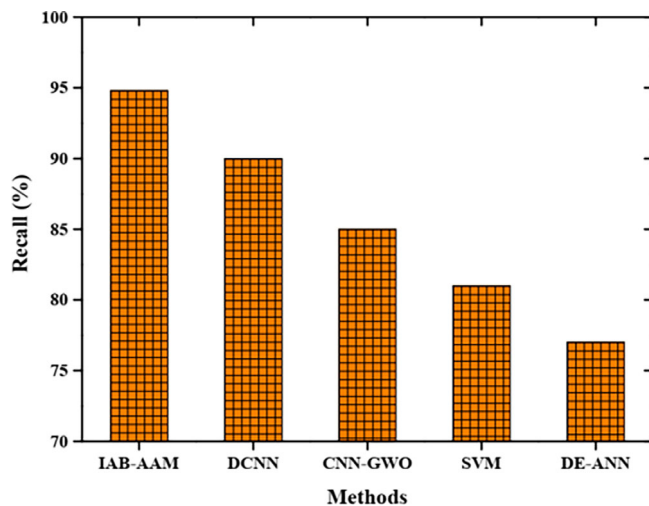


FIGURE 7 Recall analysis. CNN-GWO, convolutional neural network-based grey wolf optimization; DCNN, deep convolutional neural network; DE-ANN, differential evolution-based artificial neural network; IAB-AAM, Improved Adaboost based Aphid-Ant Mutualism; SVM, support vector machine.

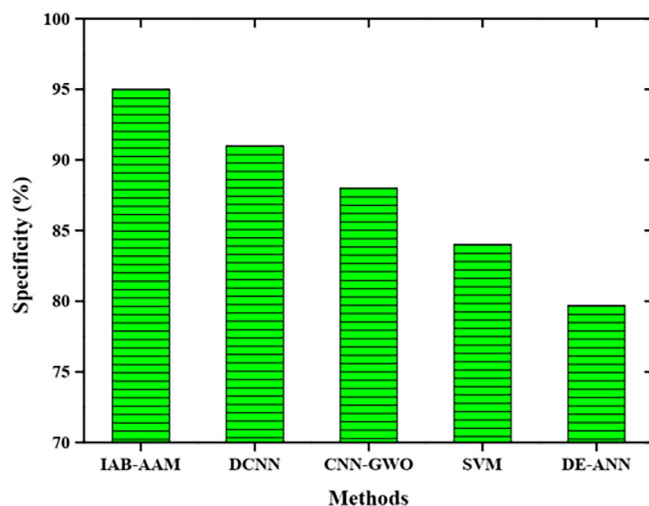


FIGURE 8 Specificity analysis. CNN-GWO, convolutional neural network-based grey wolf optimization; DCNN, deep convolutional neural network; DE-ANN, differential evolution-based artificial neural network; IAB-AAM, Improved Adaboost based Aphid-Ant Mutualism; SVM, support vector machine.

A comparative analysis of the precision rate of the proposed IAB-AAM method with various existing methods is illustrated in Figure 6. The precision of the proposed IAB-AAM method is compared with the precision of DCNN, SVM, CNN-GWO, and DE-ANN. From the analysis, skin cancer is detected and classified with higher precision of 95.4% through the proposed IAB-AAM method compared to the existing methods. A graphical result for the evaluation of the recall rate of various methods in skin cancer disease detection and classification is given in Figure 7. The recall rate of the proposed IAB-AAM method, DCNN, SVM, CNN-GWO, as well as DE-ANN is determined and analyzed. The proposed IAB-AAM method obtains a higher recall rate than the other methods. The proposed IAB-AAM method detects skin cancer and classifies them with a recall rate of 94.8%.

Figure 8 portrays the comparative analysis of specificity in detecting and classifying skin cancer through various methods. The test result demonstrates that the proposed method obtained a higher specificity compared to DCNN, SVM, CNN-GWO, and DE-ANN. The specificity of the proposed IAB-AAM method is about 95%. Table 4 describes the comparative analysis of proposed and existing methods in terms of different performance metrics. Figure 9 depicts the confusion matrix used to scale the performance of the IAB-AAM method.

Figure 10 displays the F-measure analysis of the proposed IAB-AAM method in skin cancer prediction and categorization. Compared to DCNN, SVM, CNN-GWO, and DE-ANN, the proposed IAB-AAM method attains a higher f-measure. The achieved f-measure of the proposed IAB-AAM method is 95%. In Figure 11, the graphical analysis is plotted to determine MCC for the proposed IAB-AAM approach and various other techniques namely DCNN, SVM, CNN-GWO, and DE-ANN. MCC identifies the ineffectiveness of the classifier in classifying the negative class sample. From the comparative graphical analysis, it is noted that the proposed approach attained high MMC rate of about 96% than other techniques.

Receiver operating characteristics (ROC) curve analysis of various methods for skin cancer detection and

Methods	Performance metrics (%)				
	Accuracy	Precision	Recall	Specificity	F-measure
DCNN	92.75	93	90	92	90
CNN-GWO	87.56	86.6	86	88.46	86.77
SVM	83.50	82	82	84.76	83
DE-ANN	77.90	78.32	77.5	81	77
Proposed IAB-AAM	95.7	95.4	94.8	95	95

TABLE 4 Comparative performance analysis.

Abbreviations: CNN-GWO, convolutional neural network-based grey wolf optimization; DCNN, deep convolutional neural network; DE-ANN, differential evolution-based artificial neural network; IAB-AAM, Improved Adaboost based Aphid-Ant Mutualism; SVM, support vector machine.

		Actual Value	
		Benign	Malignant
Predicted Value	Benign	1182	42
	Malignant	80	119

FIGURE 9 Confusion matrix.

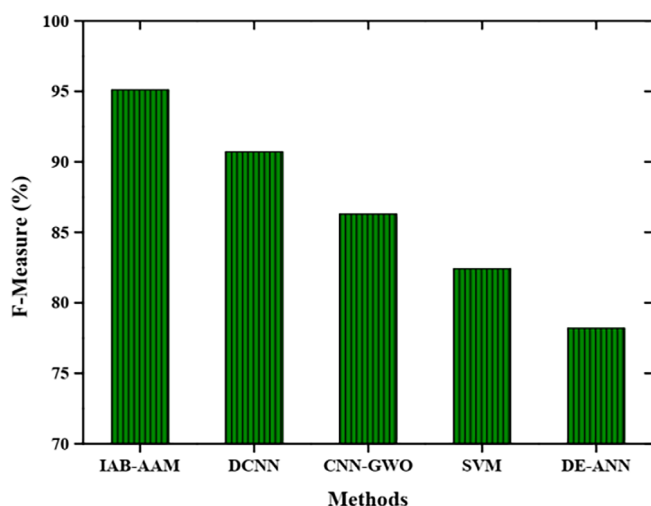


FIGURE 10 F-measure analysis. CNN-GWO, convolutional neural network-based grey wolf optimization; DCNN, deep convolutional neural network; DE-ANN, differential evolution-based artificial neural network; IAB-AAM, Improved Adaboost based Aphid-Ant Mutualism; SVM, support vector machine.

classification is graphically represented in Figure 12. The analysis reveals that the proposed IAB-AAM method offers better performance in detecting and classifying skin cancer with a higher AUC ratio differentiated from the state-of-art methods. Figure 13 portrays the performance analysis graph of proposed skin cancer classification method with and without the application of feature extraction module. From the graph, it is noted that, with the adoption of feature extractor, the accuracy rate was gained considerably. The time complexity of proposed IAB-AAM method is described in Figure 14. The time taken for processing dermoscopic images of different methods including the proposed system is given in Table 5.

5 | CONCLUSION

This paper proposes an efficient automated and intelligent skin cancer detection system to detect and classify

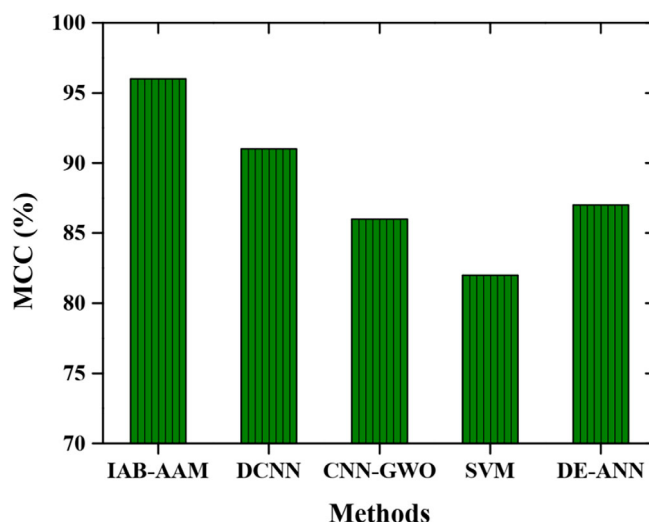


FIGURE 11 MCC analysis. CNN-GWO, convolutional neural network-based grey wolf optimization; DCNN, deep convolutional neural network; DE-ANN, differential evolution-based artificial neural network; IAB-AAM, Improved Adaboost based Aphid-Ant Mutualism; MCC, Matthews correlation coefficient; SVM, support vector machine.

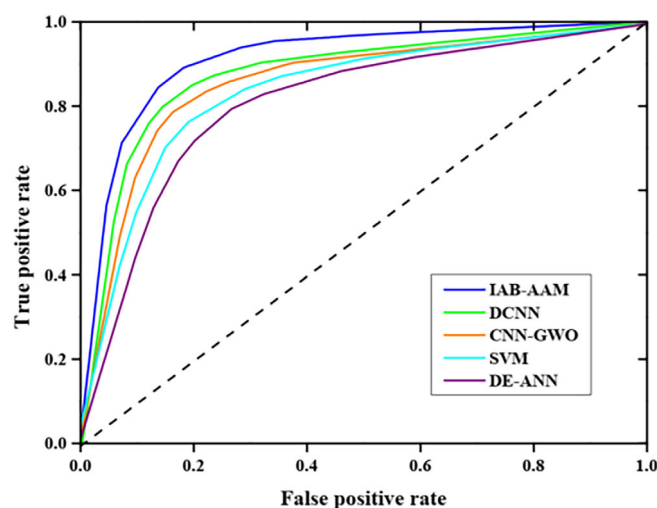


FIGURE 12 ROC curve analysis. CNN-GWO, convolutional neural network-based grey wolf optimization; DCNN, deep convolutional neural network; DE-ANN, differential evolution-based artificial neural network; IAB-AAM, Improved Adaboost based Aphid-Ant Mutualism; ROC, receiver operating characteristics; SVM, support vector machine.

the cancer classes precisely. Here, a novel IAB-AAM classification model is proposed to accurately detect and discriminate the skin cancer dermoscopic images into distinct categories (i.e., benign or malignant). The performance of the proposed method is resolved by calculating various performance metrics namely accuracy, specificity, precision, recall, f-measure, and ROC. The images for skin cancer detection and classification are obtained from

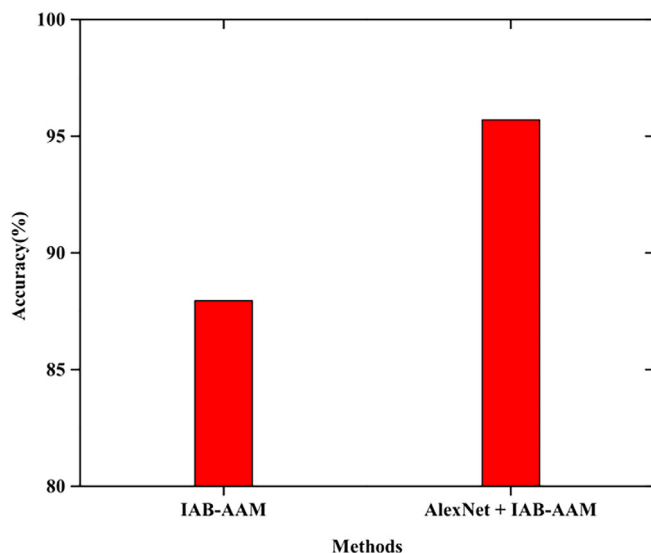


FIGURE 13 Accuracy analysis with and without AlexNet architecture. IAB-AAM, Improved Adaboost based Aphid–Ant Mutualism.

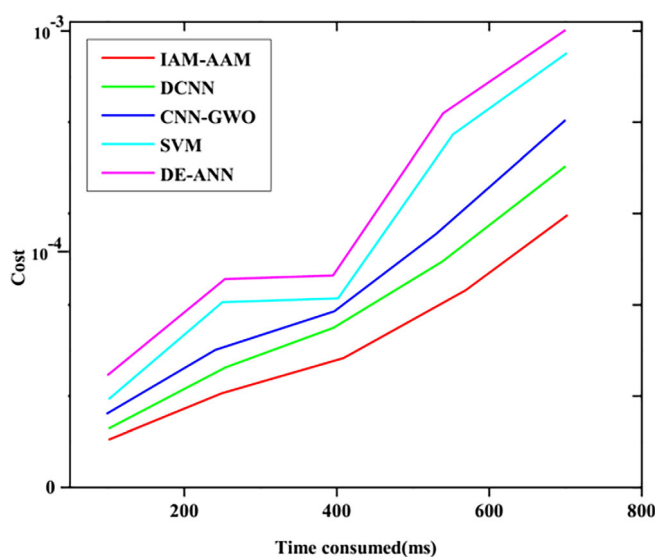


FIGURE 14 Time complexity analysis. CNN-GWO, convolutional neural network-based grey wolf optimization; DCNN, deep convolutional neural network; DE-ANN, differential evolution-based artificial neural network; IAB-AAM, Improved Adaboost based Aphid–Ant Mutualism; SVM, support vector machine.

the HAM10000 dataset. The skin cancer disease is more efficiently detected and classified through the proposed method compared to DCNN, DE-ANN, CNN-GWO, and SVM. Better accuracy and loss between testing and training are achieved through the proposed method. The proposed IAB-AAM method detects and classifies skin cancer disease with an accuracy of 95.7%. From the

TABLE 5 Computation time analysis.

Methods	Time taken/image (s)
DCNN	3.094
CNN-GWO	8.642
SVM	5.374
DE-ANN	7.346
Proposed IAB-AAM	1.725

Abbreviations: CNN-GWO, convolutional neural network-based grey wolf optimization; DCNN, deep convolutional neural network; DE-ANN, differential evolution-based artificial neural network; IAB-AAM, Improved Adaboost based Aphid–Ant Mutualism; SVM, support vector machine.

analysis, the proposed IAB-AAM method offers better performance in detecting and classifying skin cancer with higher metric rates. In the future, the proposed work will be further extended to detect various types of malignant skin cancers. In addition, the performance of detection classifier will be further improved by implementing hybrid metaheuristic approaches. Furthermore, the designed skin cancer classification system will be implemented and tested under real world scenarios.

ACKNOWLEDGMENTS

The authors would like to take this opportunity to thank the SRM Institute of Science and Technology, India, for facilitating the laboratory to carry out this research.

CONFLICT OF INTEREST STATEMENT

The authors declare no conflicts of interest.

DATA AVAILABILITY STATEMENT

The data that support the findings of this study are available from the corresponding author upon reasonable request.

ORCID

G. Renith <https://orcid.org/0000-0001-9335-6556>

A. Senthilselvi <https://orcid.org/0000-0002-0280-9773>

REFERENCES

- Goyal M, Knackstedt T, Yan S, Hassanpour S. Artificial intelligence-based image classification methods for diagnosis of skin cancer: challenges and opportunities. *Comput Biol Med.* 2020;127:104065.
- Razmjoo N, Ashourian M, Karimifard M, et al. Computer-aided diagnosis of skin cancer: a review. *Current Medical Imaging.* 2020;16(7):781–793.
- Zhang N, Cai YX, Wang YY, Tian YT, Wang XL, Badami B. Skin cancer diagnosis based on optimized convolutional neural network. *Artif Intell Med.* 2020;102:101756.
- Xu Z, Sheykahmad FR, Ghadimi N, Razmjoo N. Computer-aided diagnosis of skin cancer based on soft computing techniques. *Open Medicine.* 2020;15(1):860–871.

5. Tschandl P, Rosendahl C, Akay BN, et al. Expert-level diagnosis of non-pigmented skin cancer by combined convolutional neural networks. *JAMA Dermatol.* 2019;155(1):58-65.
6. Anderson AM, Matsumoto M, Saul MI, Secrest AM, Ferris LK. Accuracy of skin cancer diagnosis by physician assistants compared with dermatologists in a large health care system. *JAMA Dermatol.* 2018;154(5):569-573.
7. Leon R, Martinez-Vega B, Fabelo H, et al. Non-invasive skin cancer diagnosis using hyperspectral imaging for in-situ clinical support. *J Clin Med.* 2020;9(6):1662.
8. Khan MQ, Hussain A, Rehman SU, et al. Classification of melanoma and nevus in digital images for diagnosis of skin cancer. *IEEE Access.* 2019;7:90132-90144.
9. Chaturvedi SS, Tembhurne JV, Diwan T. A multi-class skin cancer classification using deep convolutional neural networks. *Multimed Tools Appl.* 2020;79(39):28477-28498.
10. Abbott LM, Smith SD. Smartphone apps for skin cancer diagnosis: implications for patients and practitioners. *Australasian Journal of Dermatology.* 2018;59(3):168-170.
11. Sankareswaran SP, Krishnan M. Unsupervised end-to-end brain tumor magnetic resonance image registration using RBCNN: Rigid transformation, B-spline transformation and convolutional neural network. *Curr Med Imaging.* 2022;18(4):387-397.
12. Dhiravidachelvi E, Senthil Pandi S, Prabavathi R, Bala Subramanian C. Artificial humming bird optimization-based hybrid CNN-RNN for accurate exudate classification from fundus images. *J Digit Imaging.* 2023;36:59-72.
13. Senthil Pandi A, Senthilselvi A, Maragatharajan M, Manju I. An optimal self adaptive deep neural network and spineker-nelled chirplet transform for image registration. *Concurrency Computat Pract Exper.* 2022;34(27):e7297.
14. Kalpana B, Reshmy AK, Senthil Pandi S, Dhanasekaran S. OESV-KRF: Optimal ensemble support vector kernel random forest based early detection and classification of skin diseases. *Biomed Signal Process Control.* 2023;85:104779.
15. Coppola D, Lee HK, Guan C. Interpreting mechanisms of prediction for skin cancer diagnosis using multi-task learning. *Proceedings of the IEEE/CVF Conference on Computer Vision and Pattern Recognition Workshops.* IEEE; 2020:734-735.
16. Vijayalakshmi MM. Melanoma skin cancer detection using image processing and machine learning. *International Journal of Trend in Scientific Research and Development (IJTSRD).* 2019;3(4):780-784.
17. Murugan A, Nair SAH, Kumar KP. Detection of skin cancer using SVM, random forest, and kNN classifiers. *J Med Syst.* 2019;43(8):1-9.
18. Göçeri E. Convolutional neural network based desktop applications to classify dermatological diseases. *2020 IEEE 4th International Conference on Image Processing, Applications and Systems (IPAS).* IEEE; 2020:138-143.
19. Das T, Kumar V, Prakash A, Lynn AM. Artificial intelligence in skin cancer: diagnosis and therapy. *Skin Cancer: Pathogenesis and Diagnosis.* Springer; 2021:143-171.
20. Khamparia A, Singh PK, Rani P, Samanta D, Khanna A, Bhushan B. An internet of health things-driven deep learning framework for detection and classification of skin cancer using transfer learning. *Trans Emerg Telecommun Technol.* 2021;32(7):e3963.
21. Kumar M, Alshehri M, AlGhamdi R, Sharma P, Deep V. A deep learning inspired skin cancer detection approach using fuzzy c-means clustering. *Mob Netw Appl.* 2020;25(4):1319-1329.
22. Tan TY, Zhang L, Neoh SC, Lim CP. Intelligent skin cancer detection using enhanced particle swarm optimization. *Knowl Based Syst.* 2018;158:118-135.
23. Dorj UO, Lee KK, Choi JY, Lee M. The skin cancer classification using deep convolutional neural network. *Multimed Tools Appl.* 2018;77(8):9909-9924.
24. Khan MA, Muhammad K, Sharif M, Akram T, de Albuquerque VHC. Multi-class skin lesion detection and classification via teledermatology. *IEEE J Biomed Health Inform.* 2021;25(12):4267-4275.
25. Mohakud R, Dash R. Designing a grey wolf optimization based hyper-parameter optimized convolutional neural network classifier for skin cancer detection. *J King Saud Univ—Computer Inf Sci.* 2021;34:6280-6291.
26. Ali MS, Miah MS, Haque J, Rahman MM, Islam MK. An enhanced technique of skin cancer classification using deep convolutional neural network with transfer learning models. *Mach Learn Appl.* 2021;5:100036.
27. Goceri E. Automated skin cancer detection: where we are and the way to the future. *2021 44th International Conference on Telecommunications and Signal Processing (TSP).* IEEE; 2021:48-51.
28. Göçeri E. Impact of deep learning and smartphone technologies in dermatology: automated diagnosis. *2020 Tenth International Conference on Image Processing Theory, Tools and Applications (IPTA).* IEEE; 2020:1-6.
29. Göçeri E. An application for automated diagnosis of facial dermatological diseases. *İzmir Katip Çelebi Üniversitesi Sağlık Bilimleri Fakültesi Dergisi.* 2021;6(3):91-99.
30. Goceri E, Karakas AA. Comparative evaluations of CNN based networks for skin lesion classification. *14th International Conference on Computer Graphics, Visualization, Computer Vision and Image Processing (CGVCVIP), Zagreb, Croatia;* 2020:1-6.
31. Aggrey ESE, Zhen Q, Kodjiku SL, et al. Detection of melanoma skin cancer using capsule network and multi-task learning framework. *2022 19th International Computer Conference on Wavelet Active Media Technology and Information Processing (ICCWAMTIP).* IEEE; 2022:1-5.
32. Goceri E. Capsule neural networks in classification of skin lesions. *International Conference on Computer Graphics, Visualization, Computer Vision and Image Processing;* 2021:29-36.
33. Goceri E. Image augmentation for deep learning based lesion classification from skin images. *2020 IEEE 4th International Conference on Image Processing, Applications and Systems (IPAS).* IEEE; 2020:144-148.
34. Goceri E. Evaluation of denoising techniques to remove speckle and gaussian noise from dermoscopy images. *Comput Biol Med.* 2022;152:106474.
35. Barata C, Marques JS, Rozeira J. A system for the detection of pigment network in dermoscopy images using directional filters. *IEEE Trans Biomed Eng.* 2012;59(10):2744-2754.
36. Gajera HK, Zaveri MA, Nayak DR. Patch-based local deep feature extraction for automated skin cancer classification. *Int J Imag Syst Technol.* 2022;32:1774-1788.

37. Ullah A, Javaid N, Asif M, Javed MU, Yahaya AS. AlexNet, AdaBoost and artificial bee Colony based hybrid model for electricity theft detection in smart grids. *IEEE Access*. 2022;10: 18681-18694.
38. Prabhakar SK, Rajaguru H. Alcoholic EEG signal classification with correlation dimension based distance metrics approach and modified Adaboost classification. *Heliyon*. 2020;6(12): e05689.
39. Eslami N, Yazdani S, Mirzaei M, Hadavandi E. Aphid-ant mutualism: a novel nature-inspired metaheuristic algorithm

for solving optimization problems. *Math Comput Simul*. 2022; 201:362-395.

How to cite this article: Renith G, Senthilselvi A. An efficient skin cancer detection and classification using Improved Adaboost Aphid-Ant Mutualism model. *Int J Imaging Syst Technol*. 2023; 1-16. doi:[10.1002/ima.22932](https://doi.org/10.1002/ima.22932)